Kerr Combs for Stimulated Brillouin Scattering Mitigation in Long-Haul Analog Optical Links

Mohammed S. Alshaykh, *Student Member, IEEE*, Yi Xuan, *Member, IEEE,* Daniel E. Leaird, Jason D. McKinney, *Senior Member, IEEE,* Minghao Qi, *Member, IEEE,* Andrew M. Weiner, *Fellow, IEEE*

***Abstract*—By limiting the optical input launch power, stimulated Brillouin scattering imposes detrimental effects on long haul analog optical links. Utilizing Kerr combs generated from an integrated Silicon Nitride microring resonator, we mitigate Brillouin scattering in a 25 Km sampled analog optical link. Such combs offer reduced footprint, high repetition rates and low power consumption, rendering them attractive for next generation integrated analog photonic links. The distribution of the optical carrier power over multiple spectral lines allows launching higher total average powers, significantly improving the link performance. Operating the link in an externally intensity-modulated direct-detection architecture, we compare link metrics using a soliton or a dark pulse as the sampling frequency comb source. An advantageous aspect of the dark pulse is its high pump conversion efficiency. We find that the Kerr comb pump conversion efficiency has a direct effect on the relative intensity noise and the link noise figure. We show that the spurious free dynamic range using Kerr combs can match that of the well-established electro-optic combs.**

***Index Terms*— Fiber optics, Four-wave mixing, Integrated optics, Kerr effect, Microwave communication, Microwave photonics, Optical resonators.**

I. Introduction

The emerging next generation cellular network (5G) revived an increasing interest in radio over fiber (RoF) solutions. To enable higher bandwidths and data rates, a shift towards new frequency bands centered at few GHz up to millimeter-Waves (>24 GHz) is being pursued. Backhauling/Fronthauling of such frequencies is a challenge, and RoF is a leading candidate. In addition to 5G networks, long haul analog optical links are of interest to a variety of applications. In radio astronomy, analog photonic links are used for antenna remoting [1] and for the distribution of local oscillator to telescopes consisting of a large number of antenna array elements [2,3]. Other applications utilizing long fiber spools include military systems [4] and a host of optical processing techniques of RF signals [5]. Many of these applications have stringent phase noise requirements rendering midspan amplification not possible. It can be shown that the link noise performance and dynamic range improve with increased optical launch power at the photodiode (average photocurrent). However, for links exceeding a few kilometers, the link input optical launch is limited by stimulated Brillouin scattering (SBS), severely degrading the link performance.

SBS is an inelastic photon-phonon interaction with a low threshold nonlinearity. Exceeding the threshold results in an avalanche increase in scattered light and saturates the output power. In single mode fiber, SBS has a narrow gain linewidth (~16 MHz) and the phonon frequency is typically ~ 11 GHz [6]. Techniques to circumvent SBS include concatenating fibers with different SBS frequencies [7], the use of few mode fibers [8] and frequency comb sources [9]. The frequency comb-based approach relies on the fact that SBS is narrowband effect. If the comb spacing exceeds the SBS gain bandwidth, the optical launch power can be increased by redistributing the average power over multiple spectral lines. As long as the power spectral density (PSD) within the SBS gain bandwidth is lower than the threshold, SBS can be mitigated. This technique allows increasing the link's optical launch power, thereby improving the RF link metrics at the expense of increased optical bandwidth.

On chip microring resonators offer an unprecedented miniaturization of optical frequency combs. The resonators' high finesse and the waveguide's narrow effective area lead to an intra-cavity resonant power buildup of high intensity tightly confined light. This paves the way to the generation of broadband optical frequency combs pumped only with a continuous-wave (CW) light source. In its early years, Kerr combs were plagued with broadband but incoherent combs. Numerous research efforts were dedicated towards studying the nonlinear dynamics and controlling it to achieve coherent and mode-locked optical frequency combs [10]. Dissipative Kerr solitons and soliton crystals have been demonstrated. In the normal dispersion regime, dark solitons, which appear as a dip

Manuscript received September xx, 2019; revised August x, 2019 and September xx, 2019; accepted September xx, 2019. Date of publication November xx, 2019; date of current version September xx, 2019. This work was supported by the U.S. Office of Naval Research. (Corresponding author: Mohammed S. Alshaykh.)

M. S. Alshaykh, Y. Xuan, D. E. Leaird, M. Qi and A. M. Weiner are with the School of Electrical and Computer Engineering, Purdue University, West Lafayette, IN 47907, USA and Birck Nanotechnology Center, Purdue University, 1205 West State Street, West Lafayette, Indiana 47907, USA (e-mail: malalsha@purdue.edu; yxuan@purdue.edu; leaird@purdue.edu; mqi@purdue.edu; amw@purdue.edu).

J. D. McKinney is with the U.S. Naval Research Laboratory, Washington, DC 20375, USA (e-mail: jason.mckinney@nrl.navy.mil).

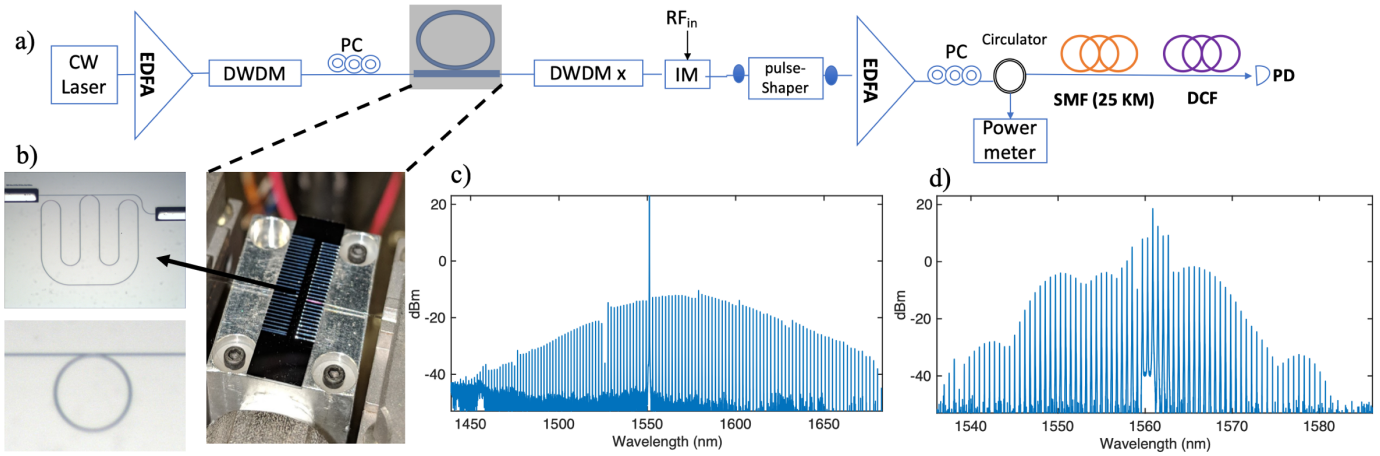

Fig. 1 a) The experimental setup:- CW: Continuous wave, EDFA: Erbium doped fiber amplifier, DWDM: Dense Wavelength Division Multiplexing Filters, IM: Intensity Modulator. SMF: Single Mode Fiber. DCF: Dispersion Compensating Fiber. (b) Microscope images of the resonator and the chip mounted on the stage. (c) The spectrum of the soliton. (d) The spectrum of the dark pulse.

in the time domain, have been demonstrated with an order of magnitude improvement in conversion efficiency [11]. As the understanding of Kerr combs is approaching maturity, their applications are increasingly expanding. Coherent digital optical communication is one example where Kerr combs have potential impact. In particular, recent experiments utilized Kerr combs for massively parallel wavelength-division multiplexing [12] and higher order 64-quadrature amplitude modulation coherent communication [13]. With growing interest in integrated RF photonics [14], analog microwave photonics, too, can benefit from Kerr combs. Recent investigations of microwave beamforming using microcomb-based true time delay networks [15-16], illustrate that integrated Kerr combs are a valuable tool for next generation analog photonic links.

In a preliminary report, we previously discussed the use of soliton Kerr combs for the mitigation of Brillouin scattering [17]. Here we provide a careful comparison of soliton and dark pulse Kerr combs for Brillouin mitigation and characterize the RF link performance. In the first demonstration of comb-based Brillouin mitigation [9], an Electro-optic frequency comb based on cascaded intensity and phase modulators was used. However, low noise and highly stable broadband Kerr combs, fabricated in CMOS compatible processes, are an attractive alternative to EO-combs for multiple reasons. Reducing the footprint is a clear advantage. Additionally, since the link is operated as a sampled analog link, Nyquist sampling must be satisfied ($f_{RF,max} < f_{rep}/2$) in order to avoid aliasing. The electro-optic comb in [9] utilized a comb with 3 GHz comb spacing, which limited the Nyquist zone to 1.5 GHz. While bandwidths up to a few tens of GHz are common for commercial modulators, the halfwave voltage (V_π) for mmWaves significantly increases even with the state-of-the-art commercial modulators. This significantly increases the power consumption which does not bode well for applications entailing a massive number of connected nodes, such as 5G and antenna remoting of telescope arrays. Recent advancements in thin film Lithium niobate (LiNbO3) are quite interesting, offering small footprints with reduced V_π and a wider RF bandwidth [18]. Nevertheless, they are still required to be driven by an amplified RF oscillator. Additionally, the bandwidth of the optical pulse scales linearly with the modulation index or RF-voltage. On the other hand, Kerr combs can have significantly larger bandwidth by engineering the dispersion, reaching an octave span [19]. Furthermore, scaling up the repetition of Kerr combs is actually easier, and combs with hundreds of GHz to 1-THz repetition rates have been achieved, enabling analog photonic links operating without aliasing at RF frequencies up to hundreds of GHz.

II. Experimental Setup

The experimental setup is shown in Fig. 1a. A continuous wave (CW) pump laser is amplified by an Erbium doped fiber amplifier (EDFA). Dense Wavelength Division Multiplexing filters (DWDM) are used to filter the ASE. Lensed fibers are used to couple in and out of the microring. Another set of DWDM filters are used after the microring to block the strong pump line. Subsequently, the generated comb is modulated by an intensity modulator (IM) which is biased at quadrature and driven by the RF signal of interest. The IM is followed by a pulse shaper and a pre-link EDFA. The pulse shaper is used for amplitude shaping and spectrum flattening. No spectral phase mask is applied. The link consists of a 25 Km spool of single mode fiber (SMF) followed by a commercial dispersion compensating fiber module (DCF). We place a circulator before the link to measure the reflected power. After the link, a photodiode (PD) converts the signal back to the electric domain.

In this paper, we use two different silicon nitride (Si_3N_4) microring resonators. The first microring resonator has a radius of 100 µm corresponding to free spectral range (FSR) of ~227.5 GHz. The ring's waveguide width is 2 µm, supporting two spatial modes, and its thickness is 790 nm leading to anomalous dispersion. The loaded quality factor of the resonance is ~1 million. The wavelength of pump laser at 1551 nm is increased to tune into the resonance from the lower wavelength side initiating a chaotic high noise comb. The detuning is increased until a single soliton is formed. The average power in the fiber before the microring was 470 mW and the total fiber to fiber

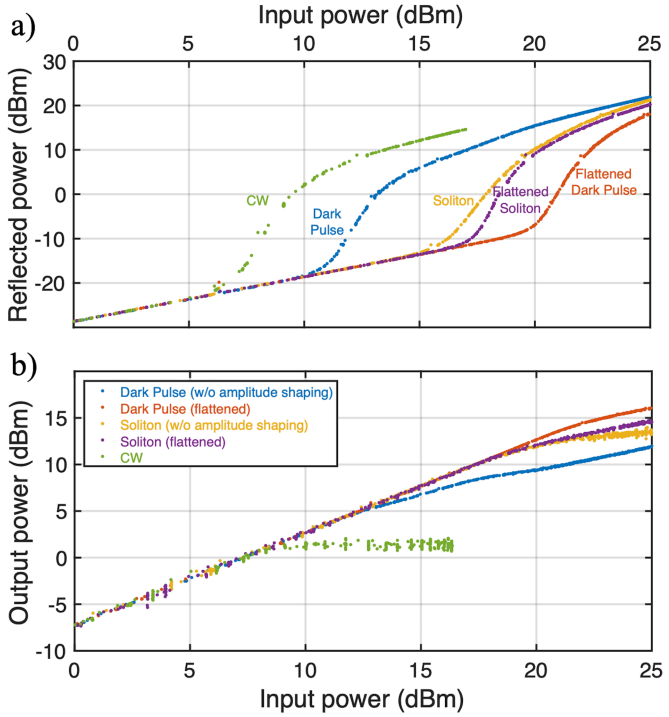

Fig. 2 (a) The reflected power and (b) the output power versus the link input power.

insertion loss was ~3.8 dB. The spectrum of the soliton directly after the microring is shown in Fig. 1(c). The soliton's spectrum has a sech^2 envelope. The shift in the center of the soliton's spectrum towards higher wavelengths is a well-known signature of Raman soliton self- frequency shift [20]. Due to the soliton's low conversion efficiency, a prominent pump line is noticeable. We can define the pump conversion efficiency (η) as

$$\eta = \frac{P_{out,comb}}{P_{in,pump}} \quad (1)$$

where $P_{in,pump}$ is the is the pump power in the input waveguide and $P_{out,comb}$ is the power of the other comb lines (i.e., excluding the pump) at the waveguide output. Note that 100% conversion efficiency corresponds to a fully depleted pump and no loss. For the single soliton, the measured pump conversion efficiency is 0.76%, which experimentally corresponds to a power of 2.5 mW in the new comb lines at the output fiber.

A second microring, with a 73 GHz FSR, is used to generate a dark pulse. The ring has a width of 2 μm and a thickness of 600 nm leading to a global normal dispersion. The pumped resonance at 1561 nm has a loaded quality factor of 1.4 million and the fiber to fiber insertion loss was ~3.8 dB. The pump is amplified to 600 mw in the fiber before the microring and tuned to generate a dark pulse that is mediated through mode interaction [21]. The pumped resonance was a single FSR away from the mode interaction region. This avoided mode crossing region shifts the resonance frequency resulting in an abrupt change in the dispersion profile which eventually leads to a local narrow anomalous dispersion region close to the pumped resonance, paving the way for the modulation instability

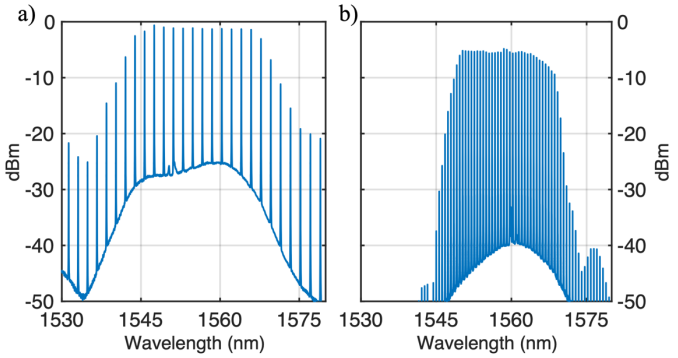

Fig. 3. The flattened spectrum of: (a) the soliton and (b) the dark pulse.

process to occur and initiate comb generation. If the resonance that is two FSRs away from the mode interaction region is pumped, we observe two FSR spaced combs being generated. This is often referred to as mode-pinning and is a typical signature of mode-interaction [22]. The dark pulse has considerably larger pump conversion efficiency: 10.31%, corresponding to 43 mw of power in the comb lines at the output fiber. The spectrum of the dark pulse directly after the microring is shown in Fig. 1(d). Note that the pump line power level is close to the newly generated comb lines. Dark pulses with even higher conversion have been achieved in [23], demonstrating 50 GHz dark pulses with 34% conversion efficiency.

III. Results

Herein, we compare the link metrics, namely: the increased SBS threshold power, the gain, third order intercept points, noise figure, relative intensity noise (RIN) and spurious free dynamic range (SFDR) for both the dark pulse and soliton with and without spectral flattening.

A. SBS Threshold Power

As mentioned earlier, Brillouin scattering is a narrowband effect. The effective SBS threshold power can be increased by redistributing the power over multiple spectral lines with a frequency spacing larger than the SBS gain bandwidth. Fig. 2 shows the average backscattered power at the reflection port of the circulator versus the link input power. With a CW input, the threshold power (P_{th}) is measured to be 6 dBm. Using the dark pulse and the soliton directly (with no flattening), the threshold power increases to 10.24 dBm and 14.88 dBm, respectively. When the spectrum is equalized to get a flatter envelope, the P_{th} of the flattened soliton increases to 16.69 dBm while the P_{th} of the flattened dark pulse increases to 19.23 dBm. The amplified flattened spectra at the link input are shown in Fig. 3. Due to the soliton's low conversion efficiency, the flattened soliton doesn't saturate the pre-link EDFA, which leads to a degraded optical signal to noise ratio (OSNR). From the acquired spectrum, we estimate that ~13.5% of the total average power is ASE. On the other hand, the ASE constitutes only ~ 0.1% of average power in the dark pulse.

The average output power at the end of the link (after the DCM in Fig. 1(a)), shown in Fig. 2, also scales with the number of spectral lines. For a CW input, the output power begins to

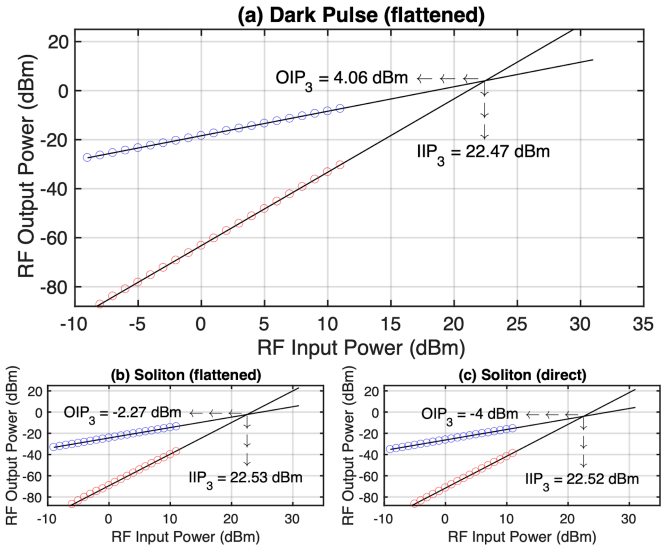

Fig. 4. Measured fundamental (blue) and IMD (red) powers at 5 GHz. The black lines are a fit to the measured data and their intersection defines the 3rd order intercept points.

saturate when the input power exceeds P_{th} by 2 to 3 dB. However, the situation differs for the other cases. Taking the direct dark pulse as an example; as the lines with stronger amplitude reach the Brillouin threshold, the weaker lines can still be amplified and pass through the link without experiencing SBS. Therefore; the output power does not saturate immediately after the P_{th}.

To predict the increase in P_{th}, ref [9] defines an effective number of lines (N) as

$$N = 1 + \frac{\Delta f_{rms}}{f_{rep}} \tag{2}$$

where Δf_{rms} is the full root-mean-square (rms) bandwidth of the comb envelope and f_{rep} is the FSR. The SBS threshold power was modeled to scale linearly with N. The prediction from this model are accurate for combs with smooth envelopes. But for non-smooth envelopes such as the direct dark pulse, the predictions are far from the measured values. Alternatively, we use a different model based on the power spectral density in which

$$\Delta P_{th}[dB] = -10 \log \alpha \tag{3}$$

where α represents the fraction of the total average power in the spectral line with maximum amplitude. This model predicts a ΔP_{th} of 4.27 dB for the Dark pulse, which agrees well with the measured 4.24 dB. For flattened spectra, this model gives results that closely agree with measured values but becomes sensitive to the optical spectrum analyzer's power accuracy and to the variations in the EDFA spectral gain distribution. On the other hand, the method based on the rms bandwidth averages out these fluctuations and gives better predictions. Table 1 summarizes the results. Note that the FSR of the soliton is ~3 times higher than the dark pulse. Ideally the comparison would be better with equivalent FSRs. However, achieving ~70 GHz cavity solitons with conventional CW pumping, while theoretically possible, is practically still challenging. The increased losses and stimulated Raman effect reduce the soliton existence range. Combined with thermal effects, these make the generation of and locking to the single soliton state challenging. An order of magnitude improvement in the quality factor – to tens of millions – can substantially expand the soliton existence range, potentially paving the way for solitons at microwave rates [24].

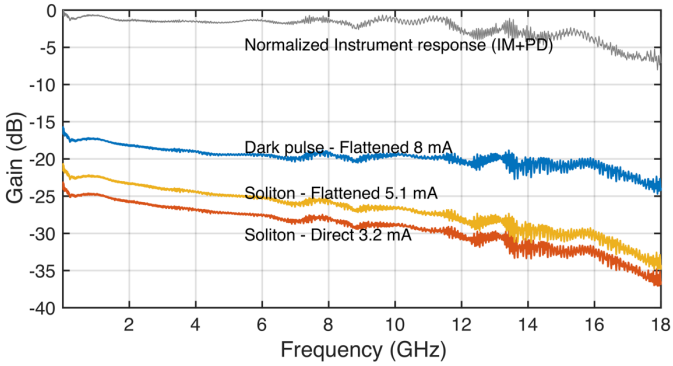

Fig. 5. The measured link RF gain.

TABLE I
INCREASE IN SBS THRESHOLD

	Measured P_{th} (dBm)	Measured ΔP_{th} (dB)	ΔP_{th} = 10 log(N)	ΔP_{th} = -10 log(α)
CW	6	-	-	-
Soliton	14.88	8.88	8.99	8.53
Soliton (flattened)	16.69	10.69	10.17	11.53
Dark Pulse	10.24	4.24	8.88	4.27
Dark Pulse (flattened)	19.23	13.23	13.24	14.21

B. *RF Gain and 3rd Order Intercept Points*

For an externally intensity-modulated direct-detection link architecture, it is well known that the gain and third order output intercept point (OIP_3) improve with increased average photocurrent (I_{dc}). By allowing higher power at the photodetector, the increased P_{th} directly improves the link performance. The links here are operated at 1-dB below the corresponding SBS threshold for each comb source used. This results in an average photocurrent of 8 mA, 5.1 mA and 3.2 mA for the flattened dark pulse, flattened soliton and direct soliton, respectively. Note that for the direct soliton, we bypass the pulse shaper to avoid the unnecessary ~ 7 dB insertion loss.

We measure the OIP_3 by the conventional two-tone test at a frequency f_1 of 5 GHz and a 2nd tone at f_2 = 5.01 GHz. The fundamental tone output versus the input RF average power is plotted in Fig. 4 alongside the 3rd order intermodulation distortion (IMD) at ($2f_2$- f_1 = 5.02 GHz). In all cases, the fundamental tone has a slope of 1 while the IMD's slope is 3 as expected. The intersection of two linear fits defines the OIP_3 and the 3rd order input intercept point (IIP_3). Theoretically, the IIP_3 depends on the modulator's frequency-dependent halfwave voltage V_π and is independent of the average photocurrent [6], and can be expressed as

$$IIP_3[dBm] = 10 \log\left(\frac{4 V_\pi^2}{R_i \pi^2}\right) + 30 \tag{4}$$

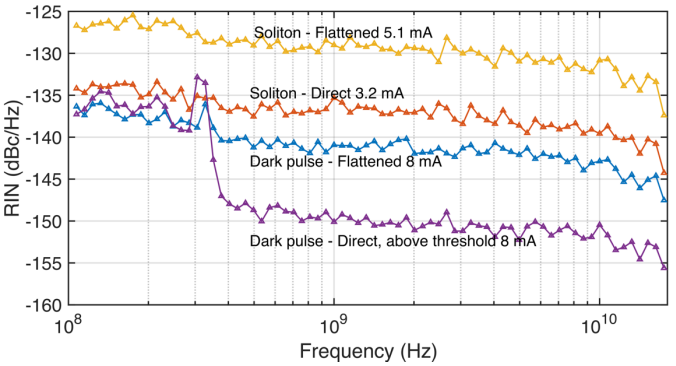

Fig. 6. The link output noise density displayed as RIN.

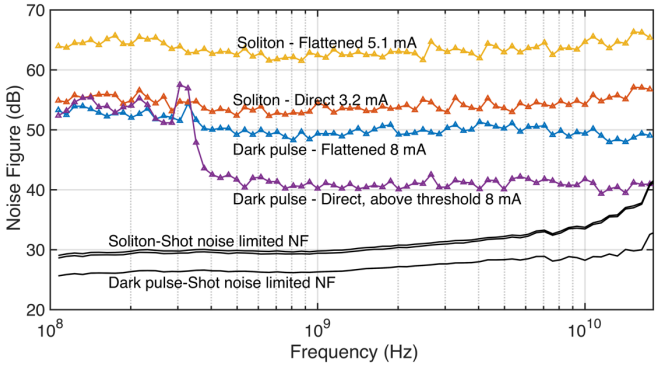

Fig. 7. The measured link noise figure.

where R_i is the input resistance of the intensity modulator (50 Ω). The OIP_3, on the other hand, depends on the average photocurrent current but not V_π, and can be found using

$$OIP_3[dBm] = 10\log(4R_oH_{pd}^2I_{dc}^2) + 30 \quad (5)$$

where R_o is the load resistance (50 Ω) and $H_{pd} = 1/2$ is the photodiode response function included to account for the matching circuit. The measured IIP_3 for all three cases is ~22.5 dBm, which is in close agreement with theoretically expected 22.08 dBm given $V_\pi = 4.46$ V. For the flattened dark pulse and the direct soliton, the measured OIP_3s of 4.1 dBm and -4 dBm are in good agreement with the theoretically expected values: 5.05 dBm and -2.9 dBm. The flattened soliton has an OIP_3 of -2.27 dBm which is 1.14 dB lower than the expected value.

The gain in an intensity-modulated direct-detection (IMDD) link is proportional to the square of I_{dc}/V_π ratio. Ref [9] shows that the same expression applies for an IMDD sampled analog link assuming the pulses at the IM are transform limited and given that any subsequent chromatic dispersion is compensated. If not compensated, chromatic dispersion can induce filtering and tapped delay line effects [25], in addition to even-order harmonic distortion [9]. The gain can be found using

$$Gain\ [dB] = 10\log\left(R_iR_o\left(\frac{\pi H_{pd}I_{dc}}{V_\pi}\right)^2\right). \quad (6)$$

Fig. 5 shows the measured link RF gain across an 18 GHz bandwidth. In sampled analog links, if larger SBS thresholds and larger RF bandwidth are needed, requiring larger optical bandwidths and larger FSRs, residual dispersion becomes important. In our setup, the commercial DCF module is designed to cancel the 2nd order dispersion but not the 3rd order dispersion. To separate the dispersion-based roll-off in gain from the instrument (IM and PD) response, we also measure and plot the normalized instrument response. The flattened and direct soliton have the same roll off profile with roughly 6 dB of additional roll off in gain at 18 GHz arising from residual dispersion. At 5 GHz, the measured -27.3 dB RF gain of the direct soliton is close to the expected -25 dB, while the flattened soliton case results in a RF gain of -25 dB, 4 dB lower than the expected theoretical value. This deviation is likely in part due to the fact that the ASE constitute a nonnegligible 13% of the total optical power, which we expect to account for a drop of 1.2 dB in gain. The rest of the roll-off is mostly due to residual dispersion. The dispersion-based gain roll-off of the dark pulse is less than the soliton due to its relatively smaller bandwidth. The dark pulse's measured response mostly follows the instrument response with a deviation of ~2.7 dB around 10 GHz. The measured gain at 5 GHz, -19.4 dB, is close to the theoretically expected -17 dB.

With increasing bandwidth (both optical and RF), more precise dispersion compensation will become desirable. This can be achieved by using dispersion compensating fiber with optimized dispersion slope. Residual higher order dispersion can be cancelled using line by line pulse shaping. Ref [26] demonstrates the ability of pulse shaping to compensate for residual higher order dispersion over a 50 Km link compressing a pulse to its transform limited duration of 500 fs, more than sufficient for microwave photonic applications. This shows that while dispersion should not be neglected, it need not be a limiting factor. Note that if the full dispersion is left uncompensated, the link then becomes essentially a comb-based RF photonic filter [25]. The Brillouin suppression effect observed here should also occur in such comb-based RF photonic filtering experiments, contributing to favorable RF metrics.

C. RIN and Noise Figure

To determine the link dynamic range and noise figure, we need to quantify the noise performance. The link noise includes contributions from thermal noise, shot noise, laser relative intensity noise and EDFA added noise. At frequencies higher than 100 MHz, the noise is typically limited by the signal-ASE beat noise. The signal-ASE beat noise decreases as the required gain of the EDFA decreases [27]. Therefore, we expect the Kerr comb conversion efficiency to have a direct effect on the noise performance. Indeed, as shown in Fig. 6, the flattened dark pulse RIN is 3 to 4.5 dB lower than that of the direct soliton. While the flattened soliton has a higher SBS threshold and gain than the direct soliton, a hefty price is paid in noise performance. The soliton's low conversion and losses arising from flattening and the pulse shaper's insertion loss leave insufficient optical power to saturate the EDFA. On average, the flattened soliton RIN is ~7.5 dB larger than the direct soliton, reaching -131 dBc/Hz at 5 GHz.

Although some links have been operated above the SBS threshold [28], the general practice - which we so far adopt - is to operate below the threshold. The rationale behind this is the following: for the CW case, as the input power is increased by a couple of dBs above the threshold, the output power is

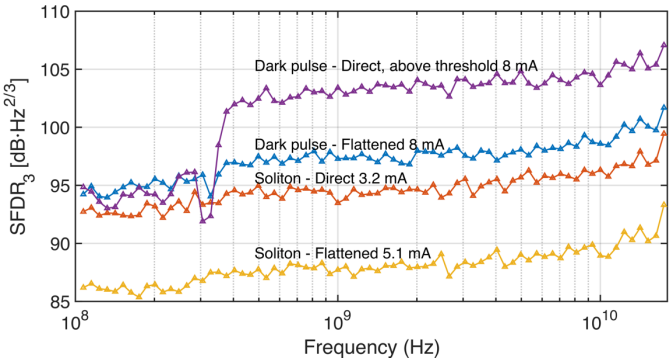

Fig. 8. The extracted spurious free dynamic range.

clamped at certain value. In other words, the loss increases; thereby increasing the noise figure. Nevertheless, this is not always the case. As previously mentioned, for a non-uniform spectrum, such as the direct dark pulse, with FSRs exceeding the narrow SBS gain bandwidth, the power of the few spectral lines exceeding the SBS threshold gets saturated, but other weaker spectral lines pass the link without experiencing SBS; thereby achieving an overall net gain. To test this, we operate the link using the direct dark pulse above the threshold. To compare it with flattened dark pulse, we operate both cases with optical powers resulting in 8 mA of average photocurrent. At frequencies lower than 300 MHz, both cases have similar RIN levels. However, the direct dark pulse RIN level decreases by 7.5 to 10 dB at frequencies higher than 400 MHz. We also notice a peak at ~ 310 MHz in the dark pulse response. Kerr combs are known to have a peak at a relaxation frequency which is on the order of the resonance linewidth [29]. Pump amplitude and phase noise conversion in Kerr combs through the four-wave-mixing (FWM) process may contribute to the noise observed below 300 MHz [30]. While not within the scope of this paper, a detailed comparison of the pump amplitude and phase noise conversion between dark pulses and solitons is of interest. Conversion of phase noise to intensity noise arising from SBS [31], which intensifies above the threshold, may be acting in concert with the pump noise conversion in Kerr combs leading to the marginal increase in the direct dark pulse RIN at lower frequencies. Additional care must be taken for the X-band when operating above the threshold. The backscattered stokes wave that is frequency-shifted by the Brillouin frequency (~11 GHz) can experience Rayleigh scattering and co-propagate with the original beam resulting in increased noise at ~11 GHz [32]. While we don't observe increased noise levels at that region, our sampling points aren't dense enough to conclusively determine its absence.

Now that we have the RF gain and noise measured, we calculate the noise figure using

$$NF = \frac{N_{tot}}{G_{RF}\, kT} \tag{7}$$

where kT represents the thermal noise contribution (k is Boltzmann's constant and T = 290 K), G_{RF} is the RF gain and N_{tot} it the electrical noise power spectral density at the link output. The results are shown in Fig. 7. The flattened soliton has a mediocre noise figure exceeding 61.5 dB across all the frequency band. The direct soliton also has flat noise figure of ~ 53.6 dB at 5 GHz; significantly higher than the shot noise limited noise figure by 21.4 dB. Note, shot noise-limited performance is typically desired in high-performance analog optical link applications. The flattened dark pulse noise figure is ~3.6 dB lower than the direct soliton. Nevertheless, this is still 21.9 dB higher than the shot noise limited noise figure. Using the direct dark pulse operated above the threshold, the NF significantly drops at high frequencies by ~13 dB. The resulting level is only 11.75 dB short above the shot noise limited noise figure at 5 GHz. Common noise cancellation using balanced detection can suppress the frequency comb's RIN. If the EDFA is placed before the modulator, the sig-ASE noise becomes common-mode and can be suppressed, potentially reducing the noise figure to the shot noise limited regime [33].

D. *Spurious Free Dynamic Range*

The SFDR is defined as the range of input powers over which the output signal power of the fundamental exceeds the output noise floor and all other third-order spurious signals (which are close to the fundamental and cannot be filtered out) are less than or equal to the noise floor [6]. The dynamic range in a quadrature-biased IMDD link is 3rd order limited. Given that the OIP_3 depends on the average photocurrent and theoretically is frequency independent, we use the measured gain and noise to calculate the $SFDR_3$ using

$$SFDR_3 = \left(\frac{OIP_3}{N_{tot}\, B_e}\right)^{\frac{2}{3}} \tag{8}$$

where B_e is the electrical bandwidth of the noise measurement (set to 1 Hz). At 5 GHz, the flattened dark pulse has a $SFDR_3$ of 98 dB·Hz$^{2/3}$, 9 dB higher than the flattened soliton. The direct dark pulse at frequencies higher than 400 MHz has the highest $SFDR_3$ and achieves a 104.8 dB·Hz$^{2/3}$ $SFDR_3$ at 5 GHz, matching the performance of the well-established electro-optic combs [9]. The $SFDR_3$ increases at high frequencies (~18 GHz) reaching 107 dB·Hz$^{2/3}$. These results constitute one of the few demonstrations of chip-based RF-photonic platforms exceeding 100 dB·Hz$^{2/3}$ SFDRs [14].

IV. Conclusion

By mitigating SBS using Kerr combs in an IMDD sampled analog optical link architecture, we demonstrate long haul transmission in a 25 Km link achieving high $SFDR_3$. The pump conversion efficiency of different Kerr combs shows a direct effect on the link noise figure. The flattened dark pulse increases P_{th} by 13.2 dB, while the direct soliton achieves a ΔP_{th} of ~10.7 dB. Although the dark pulse conversion efficiency is an order of magnitude higher than the single soliton, the losses in the flattening stage make the improvement in dynamic range smaller ($\Delta SFDR_3 \approx 2.4$ dB). While in this paper we compare single solitons and higher order dark pulses, a plethora of other Kerr comb solutions exist. In particular, the lowest order dark soliton has a smooth spectrum and a ~10% pump conversion efficiency [11]; thereby circumventing the need for a flattening

stage and potentially achieving a dynamic range equal to or exceeding ~105 dB·Hz$^{2/3}$. Higher order dark pulses with 30% conversion efficiency have been demonstrated as well [11]. If pump reject filters and the IM are integrated with the microresonator – well within reach of existing technology – the loss in the system will decrease, and the optical signal can potentially be sent directly to link operating at or slightly above threshold as demonstrated. The EDFA can then be moved after the link operating at its full power. Paired with high photocurrent handling balanced detectors, such a setup promises dramatic improvements in RF gain and dynamic range.

REFERENCES

1. S. Montebugnoli, M. Boschi, F. Perini, P. Faccin, G. Brunori, and E. Pirazzini, “Large antenna array remoting using radio-over-fiber techniques for radio astronomical application,” *Microwave and Optical Technology Letters*, vol. 46, no. 1, pp. 48–54, 2005.
2. W. Shillue, “Fiber Distribution of Local Oscillator for Atacama Large Millimeter Array,” *OFC/NFOEC 2008 - 2008 Conference on Optical Fiber Communication/National Fiber Optic Engineers Conference*, 2008.
3. Y. He, K. G. H. Baldwin, B. J. Orr, R. B. Warrington, M. J. Wouters, A. N. Luiten, P. Mirtschin, T. Tzioumis, C. Phillips, J. Stevens, B. Lennon, S. Munting, G. Aben, T. Newlands, and T. Rayner, “Long-distance telecom-fiber transfer of a radio-frequency reference for radio astronomy,” *Optica*, vol. 5, no. 2, p. 138, 2018.
4. G. Tavik, C. Hilterbrick, J. Evins, J. Alter, J. Crnkovich, J. D. Graaf, W. Habicht, G. Hrin, S. Lessin, D. Wu, and S. Hagewood, “The advanced multifunction RF concept,” *IEEE Transactions on Microwave Theory and Techniques*, vol. 53, no. 3, pp. 1009–1020, 2005.
5. R. A. Minasian, “Ultra-Wideband and Adaptive Photonic Signal Processing of Microwave Signals,” *IEEE Journal of Quantum Electronics*, vol. 52, no. 1, pp. 1–13, 2016.
6. V. J. Urick, J. D. McKinney, and K. J. Williams, *Fundamentals of Microwave Photonics*, Hoboken, NJ, USA: Wiley, 2015.
7. C. A. S. D. Oliveira, C.-K. Jen, A. Z. Shang, and C. Saravanos, “Stimulated Brillouin scattering in cascaded fibers of different Brillouin frequency shifts,” *Fiber Laser Sources and Amplifiers IV*, 1993.
8. H. Wen, H. Zheng, Q. Mo, A. M. Velázquez-Benítez, C. Xia, B. Huang, H. Liu, H. Yu, P. Sillard, J. E. A. Lopez, R. A. Correa, and G. Li, “Few-mode fibre-optic microwave photonic links,” *Light: Science & Applications*, vol. 6, no. 8, 2017.
9. J. D. Mckinney, V. J. Urick, and J. Briguglio, “Optical Comb Sources for High Dynamic-Range Single-Span Long-Haul Analog Optical Links,” *IEEE Transactions on Microwave Theory and Techniques*, vol. 59, no. 12, pp. 3249–3257, 2011.
10. T. J. Kippenberg, A. L. Gaeta, M. Lipson, and M. L. Gorodetsky, "Dissipative Kerr solitons in optical microresonators," *Science*, vol. 361, no. 6402, eaan8083, 2018.
11. X. Xue, P.-H. Wang, Y. Xuan, M. Qi, and A. M. Weiner, “Microresonator Kerr frequency combs with high conversion efficiency,” *Laser & Photonics Reviews*, vol. 11, no. 1, p. 1600276, 2017.
12. P. Marin-Palomo, J. N. Kemal, M. Karpov, A. Kordts, J. Pfeifle, M. H. P. Pfeiffer, P. Trocha, S. Wolf, V. Brasch, M. H. Anderson, R. Rosenberger, K. Vijayan, W. Freude, T. J. Kippenberg, and C. Koos, “Microresonator-based solitons for massively parallel coherent optical communications,” *Nature*, vol. 546, no. 7657, pp. 274–279, 2017.
13. A. Fülöp, M. Mazur, A. Lorences-Riesgo, Ó. B. Helgason, P.-H. Wang, Y. Xuan, D. E. Leaird, M. Qi, P. A. Andrekson, A. M. Weiner, and V. Torres-Company, “High-order coherent communications using mode-locked dark-pulse Kerr combs from microresonators,” *Nature Communications*, vol. 9, no. 1, 2018.
14. D. Marpaung, J. Yao, and J. Capmany, “Integrated microwave photonics,” *Nature Photonics*, vol. 13, no. 2, pp. 80–90, 2019.
15. X. Xue, Y. Xuan, C. Bao, S. Li, X. Zheng, B. Zhou, M. Qi, and A. M. Weiner, “Microcomb-Based True-Time-Delay Network for Microwave Beamforming With Arbitrary Beam Pattern Control,” *Journal of Lightwave Technology*, vol. 36, no. 12, pp. 2312–2321, 2018.
16. X. Y. Xu et al., “Photonic microwave true time delays for phased array antennas using a 49 GHz FSR integrated optical micro-comb source,” *Photon. Res.*, vol. 6, no. 5, pp. B30–B36, May 2018.
17. M. S. Alshaykh, Y. Xuan, D. E. Leaird, J. D. Mckinney, M. Qi, and A. M. Weiner, “Kerr Combs for Single-Span Long-Haul Analog Optical Links,” in *2018 IEEE Photonics Conference (IPC)*, Reston, VA, 2018, pp. 1-2.
18. C. Wang, M. Zhang, X. Chen, M. Bertrand, A. Shams-Ansari, S. Chandrasekhar, P. Winzer, and M. Lončar, “Integrated lithium niobate electro-optic modulators operating at CMOS-compatible voltages,” *Nature*, vol. 562, no. 7725, pp. 101–104, 2018.
19. D. T. Spencer et al., "An optical-frequency synthesizer using integrated photonics." *Nature*, vol. 557, no. 7703, pp. 81-85, 2018.
20. C. Bao, Y. Xuan, C. Wang, J. A. Jaramillo-Villegas, D. E. Leaird, M. Qi, and A. M. Weiner, “Soliton repetition rate in a silicon-nitride microresonator,” *Optics letters,* vol. 42, no. 4, pp. 759–762, 2017.
21. X. Xue, Y. Xuan, Y. Liu, P.-H. Wang, S. Chen, J. Wang, D. E. Leaird, M. Qi, and A. M. Weiner, “Mode-locked dark pulse Kerr combs in normal-dispersion microresonators,” *Nature Photonics*, vol. 9, no. 9, pp. 594–600, 2015.
22. X. Xue, M. Qi, and A. M. Weiner, “Normal-dispersion microresonator kerr frequency combs,” *Nanophotonics*, vol. 5, no. 2, pp. 244–262, 2016.
23. C. Wang, C. Bao, Y. Xuan, K. Han, D. E. Leaird, M. Qi, and A. M. Weiner, “Normal dispersion high conversion efficiency kerr comb with 50 GHz repetition rate,” in *CLEO: Science and Innovations*. Optical Society of America, 2017, pp. SW4N–5.
24. M. H. P. Pfeiffer, J. Liu, A. S. Raja, T. Morais, B. Ghadiani, and T. J. Kippenberg, “Ultra-smooth silicon nitride waveguides based on the Damascene reflow process: fabrication and loss origins,” *Optica*, vol. 5, no. 7, p. 884, 2018.
25. E. Hamidi, D. E. Leaird, and A. M. Weiner, “Tunable programmable microwave photonic filters based on an optical frequency comb,” *IEEE Trans. Microw. Theory Tech.*, vol. 58, no. 11, pp. 3269–3278, Nov. 2010.
26. Z. Jiang, S.-D. Yang, D. E. Leaird, and A. M. Weiner, “Fully dispersion-compensated 500 fs pulse transmission over 50 km single-mode fiber,” *Optics letters*, vol. 30, no. 12, pp. 1449–1451, 2005.
27. A. W. S. Putra, M. Yamada, H. Tsuda, and S. Ambran, “Theoretical analysis of noise in erbium doped fiber amplifier,” IEEE J. Quantum Electron., vol. 53, no. 4, Aug. 2017, Art. no. 5100108.
28. P. S. Devgan, V. J. Urick, K. J. Williams and J. F. Diehl, "Long-haul microwave analog link with shot-noise-limited performance above the Stimulated Brillouin Scattering threshold," *2008 International Topical Meeting on Microwave Photonics jointly held with the 2008 Asia-Pacific Microwave Photonics Conference*, Gold Coast, Qld, 2008, pp. 326-329.
29. A. B. Matsko and L. Maleki, “Feshbach resonances in Kerr frequency combs,” *Physical Review A*, vol. 91, no. 1, 2015.
30. A. B. Matsko and L. Maleki, “Noise conversion in Kerr comb RF photonic oscillators,” *Journal of the Optical Society of America B*, vol. 32, no. 2, p. 232, 2015.
31. J. Zhang and M. R. Phillips, "Modeling intensity noise caused by stimulated Brillouin scattering in optical fibers," in *Proc. Conf. Lasers Electro-Opt. Dig.*, May 2005, pp. 140-142, Paper CMH6.
32. V. J. Urick, P. F. Knapp, L. Swingen, M. S. Rogge, A. L. Campillo, F. Bucholtz, and J. L. Dexter, “Design and Characterization of Long-Haul Single-Channel Intensity-Modulated Analog Fiber-Optic Links,” *NRL Memorandum Report*, NRL/MR/5650-05-8904, 2015.
33. H.-J. Kim, D. E. Leaird, A. J. Metcalf, and A. M. Weiner, “Comb-Based RF Photonic Filters Based on Interferometric Configuration and Balanced Detection,” *Journal of Lightwave Technology*, vol. 32, no. 20, pp. 3478–3488, 2014.